LISA Parameter Estimation Using Numerical Merger Waveforms

J.I. Thorpe, S.T. McWilliams, B.J. Kelley, R.P. Fahey, K. Arnaud, and J.G. Baker

NASA Goddard Space Flight Center, 8800 Greenbelt Rd., Greenbelt, MD 20771, USA

E-mail: James.I.Thorpe@nasa.gov

Abstract. Coalescing supermassive black holes are expected to provide the strongest sources for gravitational radiation detected by LISA. Recent advances in numerical relativity provide a detailed description of the waveforms of such signals. We present a preliminary study of LISA's sensitivity to waveform parameters using a hybrid numerical/analytic waveform describing the coalescence of two equal-mass, non-spinning black holes. The *Synthetic LISA* software package is used to simulate the instrument response and the Fisher information matrix method is used to estimate errors in the waveform parameters. Initial results indicate that inclusion of the merger signal can significantly improve the precision of some parameter estimates. For example, the median parameter errors for an ensemble of systems with total redshifted mass of $10^6\,\mathrm{M}_\odot$ at a redshift of $z \sim 1$ were found to decrease by a factor of slightly more than two when the merger was included.

1. Introduction

The inspiral and merger of massive black hole binaries (MBHBs) are expected to produce the strongest gravitational wave (GW) signals in the LISA frequency band[1]. The large signal-to-noise ratios (SNRs) of these signals will allow LISA to move beyond the simple detection of GWs into the rich field of parameter estimation. By extracting parameters such as mass, mass ratio, spins, luminosity distance, and location LISA will provide information that will shed light on a wealth of astrophysical questions. Examples include testing models of hierarchical structure formation through MBHB merger trees[2] and, if electromagnetic counterparts to MBHB mergers can be found, constraining cosmology through direct measurements of the distance-redshift relationship at high redshifts[3].

Estimates of the accuracy of LISA's extracted parameters have been developing for the past several years. Much of this work has paralleled progress in describing the waveforms from MBHBs. Initial studies focused on equal-mass, non-spinning holes[4], while later analyses have added the effects of spin[5, 6] and higher harmonics[7]. One things all of these works have in common is that they do not include the final merger/ringdown portion of the MBHB waveform. This is in part due to expectation

that LISA's sensitivity to certain parameters arises from modulations caused by the orbit of the constellation and that the merger signals, while strong, are too short-lived to experience any such modulations. The other, more practical reason why the merger has been excluded is that the post-Newtonian (PN) approximations used to compute the waveforms break down at or near the merger and do not give an accurate description of the waveform.

Numerical relativity (NR) has now answered the question of what the merger portion of the waveform looks like[8, 9], at least for a restricted set of parameters. Analyses using hybrid PN/NR waveforms confirm that the merger portion of the signal often dominates the total SNR of a LISA MBHB observation[10]. However, an increase in SNR does not necessarily result in an increase in parameter sensitivity. In particular, the classic mechanism of orbit-induced modulations should play a limited role for merger signals. There may, however, be other ways in which the merger can contribute. In this paper we present an initial study of LISA parameter estimation using complete waveforms for equal-mass, non-spinning MBHBs.

The remainder of the paper is organized as follows. In section 2, we describe the method used to perform the sensitivity calculation, including details on the waveform (2.1), the instrument model (2.2), and the parameter sensitivity computation (2.3). In section 3 we present results of our calculation for two ensembles of systems with different mass ranges. In section 4 we compare our results with those of previous estimates and discuss their implications.

2. Methodology

2.1. Waveform

The waveform used in these parameter estimation studies is a hybrid of PN and NR waveforms as described in section IV of Baker, et al.[10]. The merger and ring-down portions are simulated numerically using the moving-puncture method with radiation extracted as amplitudes of spin-weighted spherical harmonics at fixed extraction radii. In this work we consider only equal-mass, non-spinning MBHBs and retain only the quadrupolar ($l = |m| = 2$) modes on grounds of symmetry. The numerical simulation begins approximately $1200\,M_{rest}$ before merger, where M_{rest} is the total mass of the system in the rest frame prior to radiation losses. This corresponds to approximately seven orbits prior to merger. Early parts of the signal, beginning approximately $2 \times 10^5\,M_{rest}$ before merger, are modeled using a PN waveform with a 3.5PN order in phase and a 2.5PN order in amplitude. The two waveforms are matched at the point where the estimated accuracy of the numerical simulation first surpasses the estimated accuracy of the PN waveform, in this case at a time of $328M_{rest}$ before merger. The sampling cadence of the hybrid waveform is $1\,M_{rest}$.

Since the hybrid waveform relies on numerical simulations to generate the merger segment it is not practical to use this technique to generate the large sets of waveforms

with varying parameters that are needed for data analysis. If, however, we restrict ourselves to variations in extrinsic parameters only, it is possible to use a single "master" waveform and vary the extrinsic parameters using analytic formulae.

For our purposes, the desired waveforms are dimensionless strain in the Solar System Barycenter (SSB). These depend on six extrinsic parameters: the redshifted total system mass $M = M_{rest}(1+z)$, luminosity distance D_L, coalescence time t_c, and three angles describing the orientation of the binary, in this case an inclination ι, initial orbital phase ϕ_o, and a polarization ψ. If we define a "complex" strain $\tilde{h} \equiv h_+ + ih_\times$, we can use the following relationship between the strain in the source frame, $\tilde{h}_{source}$, and the strain in the SSB, $\tilde{h}_{SSB}$:

$$\tilde{h}_{SSB} = \sqrt{\frac{5}{4\pi}}\frac{G}{c^2}\frac{M}{D_L}e^{i\psi}\left[\tilde{h}_{source}\cos^4\left(\frac{\iota}{2}\right)e^{2i\phi_o} + \tilde{h}^*_{source}\sin^4\left(\frac{\iota}{2}\right)e^{-2i\phi_o}\right] \quad (1)$$

Two additional extrinsic parameters describe the sky location of the binary in the SSB frame. In this case we use galactic longitude Φ and latitude Θ. The effect of these parameters of the waveform is handled by the instrument model, described in the next section. In total, there are eight extrinsic parameters which determine the SSB waveform from the master source waveform. For convenience, we use the vector $\vec{\lambda} \equiv (M, D_L, \Theta, \Phi, \iota, \phi_o, \psi, t_c)$ to denote the extrinsic parameters of a particular system and use the shorthand notation $\tilde{h} = \tilde{h}(\vec{\lambda})$ to represent the transformation in (1) .

2.2. Instrument Model

There are two necessary components for modeling the sensitivity of a gravitational wave detector[11]: a response function relating the gravitational wave signal to the instrument output and a noise model describing all other components of the instrument output.

In the case of LISA, the instrument outputs are the Time Delay Interferometry[12] (TDI) streams. TDI is a technique by which the differential phase measurements made at each spacecraft are combined with appropriate time delays in order to form outputs for which laser phase noise is canceled but GW signals remain. Many variants of TDI have been described in the literature[13]. For data analysis purposes, it is convinient to use a set of "optimal" TDI channels[14] that form an orthongonal basis in the TDI signal space. Such a set of channels has the property that the noises in the channels are independent and each channel can therefore be treated as a separate detector. Prince, et al.[14] defined a set of optimal TDI channels, (A, E, T) which were formed from the so-called TDI "generators", (α, β, γ). We have selected a modified version of (A, E, T) based on the first-generation Michelson TDI variables (X, Y, Z):

$$\begin{aligned} A' &= \frac{1}{2}\frac{1}{\sqrt{2}}(Z - X), \\ E' &= \frac{1}{2}\frac{1}{\sqrt{6}}(Z + X - 2\cdot Y), \\ T' &= \frac{1}{2}\frac{1}{\sqrt{3}}(Z + X + Y). \end{aligned} \quad (2)$$

The pre-factor of 1/2 is chosen so that (A', E', T') reduce to (A, E, T) in the low frequency limit. For brevity, we will denote the set of three *modified* optical channels by the vector $\mathbf{A} \equiv (A', E', T')$.

2.2.1. Response to Signals The response function of a particular TDI channel depends on the detector geometry and its orientation relative to the source. These quantities evolve as the LISA constellation orbits the Sun, causing modulations in the response which provide a potential mechanism for discerning source parameters such as sky position. For GW frequencies below about 5 mHz, corresponding to wavelengths larger than the size of the detector, it is possible to factor out a fixed detector response from the orbital modulation, which can then be treated analytically[4]. When higher GW frequencies are of interest, which will generally be the case when the merger and/or higher harmonics are included, the effect of the evolving detector geometry will become important.

For this work, we have chosen to use the *Synthetic LISA* software package[15] to model the instrument response to the GW signal. *Synthetic LISA* models the orbits of the individual spacecraft and computes the constellation geometry. The GW response in each arm is then computed and assembled to form the appropriate TDI combinations.

2.2.2. Response to Noise It would of course be possible to use *Synthetic LISA* to compute the noise output in the **A** channels as well as the signal response. Simulated noise with appropriate spectral and statistical properties would be injected at each measurement point and propagated just as the GW signal response is. The difficulty with this approach is that statistical variations cause the noise curve to change from one run to the next, washing out the subtle changes corresponding to variations in waveform parameters. This effect can be mitigated by averaging repeated simulations with varying seeds, however this adds computational cost to the instrument model.

The alternative approach, the one taken by most estimates of LISA sensitivity in the literature, is to derive an analytic expression for the average noise level in a TDI channel given the noise spectra of the individual components[13]. For **A**, the one-sided power-spectral densities (PSDs) of the noise are given by the following expressions

$$\begin{aligned} S_{A'} = S_{E'} &= 2\sin^2(2\pi fL/c) \cdot \{2 \cdot [3 + 2\cos(2\pi fL/c) + \cos(4\pi fL/c)]\, S_{pm}(f) \\ &+ \; [2 + \cos(2\pi fL/c)]\, S_{op}(f)\} \\ S_{T'} &= 8\sin^2(2\pi fL/c) \cdot \sin^2(\pi fL/c) \cdot \left[4\sin^2(\pi fL/c)\, S_{pm}(f) + S_{op}(f)\right] \end{aligned} \tag{3}$$

where L is the average arm length of the constellation, f is the Fourier frequency, and $S_{pm}(f)$ and $S_{op}(f)$ are the strain-equivalent proof-mass acceleration and optical-path noises of the LISA links respectively. For this work, the following expressions were used to describe $S_{pm}(f)$ and $S_{op}(f)$,

$$\begin{aligned} S_{pm}(f) &= \left(2.5 \times 10^{-48}\right) (f/1\,\mathrm{Hz})^{-2} \cdot \sqrt{1 + (f/0.1\,\mathrm{mHz})^{-4}} \\ S_{op}(f) &= 1.8 \times 10^{-37}\, (f/1\,\mathrm{Hz})^{2}\,. \end{aligned} \tag{4}$$

In addition to the noise introduced by the instrument, MBHB signals are also partially obscured by a "foreground" of other GW signals. This foreground is composed of a superposition of tens of thousands of compact binaries in our galaxy and its neighborhood. Using the expression for displacement noise derived by Timpano, Rubbo, and Cornish[16], the noise contribution in the Michelson (X, Y, Z) TDI channels of this stochastic foreground can be estimated as

$$S_{gal}(f) = \left[\frac{8\pi L f}{c}\sin\left(\frac{2\pi L f}{c}\right)\right]^2 \cdot G(f) \tag{5}$$

$$G(f) \equiv \begin{cases} 10^{-44.62}(f/1\,\mathrm{Hz})^{-2.3}, & 10\,\mu\mathrm{Hz} \le f < 1\,\mathrm{mHz} \\ 10^{-50.92}(f/1\,\mathrm{Hz})^{-4.4}, & 1\,\mathrm{mHz} \le f < 2\,\mathrm{mHz} \\ 10^{-62.8}(f/1\,\mathrm{Hz})^{-8.8}, & 1\,\mathrm{mHz} \le f < 4\,\mathrm{mHz} \\ 10^{-89.68}(f/1\,\mathrm{Hz})^{-20}, & 4\,\mathrm{Hz} \le f < 10\,\mathrm{mHz} \end{cases} \tag{6}$$

In this work we have made the assumption that $S_{gal}(f)$ enters the A' and E' channels with the same transfer function as the (X, Y, Z) channels and that it is not present in the $T^{'}$ channel. The total instrument noise in the **A** channels is given by the expressions in (3) with the component noises in (4) and the galactic foreground noise in (5) added to the A' and E' channels.

2.2.3. Hazards of Hybrid Instrument Models Combining a numerical instrument response model with an analytic noise model must be done with some care in order to avoid certain hazards. Consider computing the SNR of a particular GW signal using *Synthetic LISA* to estimate the detector response and the analytic formulas in (3) to compute the noise. The analytic formulas predict that the noise will go to zero at the null frequencies $f_n = nc/L$, where $n = 1, 2, 3....$ This perfect cancellation only occurs because the arm lengths are exactly equal and are static. Were such a model used to compute the signal response, it too would go to zero for $f = f_n$. However, when *Synthetic LISA* computes the signal response, the cancellation is not perfect and some signal is still present at $f = f_n$. This results in an infinite contribution to the SNR at $f = f_n$. Even if *Synthetic LISA* is modified to use an equal-arm rigid detector, the power-spectrum of the signal must still be estimated from the discrete time series, an imperfect process in which power in neighboring bins can leak into the bins corresponding to $f = f_n$, again leading to infinite SNR. To alleviate this problem, we added an artificial "floor" to each of the noise spectra in (3) of $10^{-40}(f/1\,\mathrm{Hz})^2$.

The T' channel has a related problem at low frequencies, where the expression in (3) can be reduced to $S_{T'}(f) \approx (6.60 \times 10^{-44})(f/1\,\mathrm{Hz})^2$ assuming the noise levels in (4). The corresponding signal response function should also fall off with f^2 at low frequencies in order for SNR to converge. In practice, the T' channel response for our signals leveled off at a finite value. This caused an erroneous increase in SNR (and parameter sensitivity) from the low-frequency portion of the T' channel. The exact reason for this flooring behavior is not clear, it may be due to asymmetries in or motion of the constellation or simply from errors in the estimation of signal power spectra. It may be possible to

address the problem with the T' channel by adding an artificial noise floor to $S_{T'}(f)$ or by only using it in the high-frequency limit. For this work, however, we have chosen to neglect the contributions of the T' channel until the issue can be further investigated.

2.3. Parameter Sensitivity Calculation

With the waveform described in 2.1 and the instrument model described in 2.2 in hand, the next step is to develop a procedure for evaluating parameter sensitivity. Like many others in the community, we have selected the Fisher information matrix approach because of its relative simplicity and speed. The steps for the approach are as follows. A SSB waveform with a particular set of extrinsic parameters $\vec{\lambda}_o$ is generated from the master waveform,

$$\tilde{h}_o = \tilde{h}\left(\vec{\lambda}_o\right) \tag{7}$$

A set of perturbed waveforms is then generated by perturbing each of the parameters individually,

$$\tilde{h}_i = \tilde{h}(\vec{\lambda}_o + \delta\lambda_i\hat{i}), \tag{8}$$

where $\delta\lambda_i$ is the size of the perturbation in the $\hat{i}$ parameter direction. The instrument response to the original waveform and each of the perturbed waveforms is calculated using *Synthetic LISA*. The partial derivative of the instrument response with respect to each parameter is then estimated using a one-sided difference,

$$\left.\frac{\partial \mathbf{A}}{\partial \lambda^i}\right|_{\vec{\lambda}=\vec{\lambda}_o} \approx \frac{\mathbf{A}_i - \mathbf{A}_o}{\delta\lambda_i} \tag{9}$$

where $\mathbf{A}_o$ is the response to $\tilde{h}_o$ and $\mathbf{A}_i$ is the response to $\tilde{h}_i$. These parameter derivatives are used to estimate the Fisher information matrix

$$\mathbf{\Gamma}_{ij} = \left(\frac{\partial \mathbf{A}}{\partial \lambda^i}\middle|\frac{\partial \mathbf{A}}{\partial \lambda^j}\right) \tag{10}$$

where $(a|b)$ denotes the noise-weighted inner product,

$$(a|b) \equiv 2\int_0^\infty \frac{a^\star(f)b(f) + a(f)b^\star(f)}{S_n(f)}df. \tag{11}$$

The quantity $S_n(f)$ is the PSD of the appropriate TDI channel, including the foreground as described in (2.2.2). In our case we estimate the Fourier transform of $\partial\mathbf{A}/\partial\lambda^i$ from the time series using a discrete Fourier transform with tapering applied to the early and late portion of the signal to reduce spectral artifacts. The inner product in (11) is evaluated as a discrete sum with finite upper and lower integration limits.

Since the $\mathbf{A}$ channels are constructed to be linearly independent, it is appropriate to sum their individual Fisher matrices to yield the effective Fisher matrix for the instrument as a whole. However, as discussed in section 2.2.2, the T' channel was not well-behaved in our instrument model. For that reason, we have omitted the T' channel and defined the composite Fisher matrix as

$$\Gamma_{ij} = \Gamma_{ij}^{(A')} + \Gamma_{ij}^{(E')}. \tag{12}$$

Table 1. Mean ($\Delta\bar{\lambda}^i$) and median ($\Delta\tilde{\lambda}^i$) values for parameter errors and SNR for an ensemble of 140 equal-mass, non-spinning binaries with $M = 10^6\,\mathrm{M}_\odot$ at $D_L = 6\,\mathrm{Gpc}$ ($z \sim 1$). For the 'pre-ISCO' case, the integration of Fisher matrix elements was cutoff at a frequency corresponding to the Schwarzchild ISCO. The 'total' case includes the entire waveform.

λ^i	$\Delta\bar{\lambda}^i$ (total)	$\Delta\bar{\lambda}^i$ (pre-ISCO)	$\Delta\tilde{\lambda}^i$ (total)	$\Delta\tilde{\lambda}^i$ (pre-ISCO)
SNR_{AE}	1.12×10^3	8.35×10^2	9.28×10^2	6.98×10^2
$\ln(M/M_\odot)$	2.35×10^{-6}	4.00×10^{-6}	1.66×10^{-6}	3.26×10^{-6}
$\ln(D_L/1\,\mathrm{pc})$	3.78×10^{-1}	6.07×10^{-1}	4.48×10^{-2}	1.18×10^{-1}
Θ (deg)	3.84	7.19	2.15	5.28
Φ (deg)	17.7	26.9	4.64	9.19
ι (deg)	81.9	137	1.08	3.12
ϕ_o (deg)	607	1270	1.59	4.26
ψ (deg)	620	1290	7.46	15.9
t_c(sec)	17.1	39.5	6.87	27.3

In the limit of large SNR, the covariance matrix is simply the inverse of the covariance matrix. Using this limit, we estimate the covariance matrix Σ^{ij} and parameter errors $\Delta\lambda^i$ in the standard fashion

$$\Sigma^{ij} = (\Gamma^{-1})^{ij}, \tag{13}$$

$$\Delta\lambda^i = \sqrt{\Sigma^{ii}}, \tag{14}$$

These quantities are valid for a system with the particular set of parameters $\vec{\lambda}_o$. It is widely recognized that Σ^{ij} can depend heavily on the particular choice of $\vec{\lambda}_o$. To explore this dependence, a Monte Carlo approach is taken whereby $\vec{\lambda}_o$ is varied and Σ^{ij} is computed for each system. This yields an estimate of the probability distribution function for Σ^{ij} and $\Delta\lambda^i$.

3. Results

For our initial trials, we choose an ensemble of 140 systems, each with $M = 10^6\,\mathrm{M}_\odot$ and $D_L = 6\,\mathrm{Gpc}$, corresponding to $z \sim 1$ in standard Λ-CDM cosmology. The remaining parameters (Θ, Φ, ι, ϕ_o, ψ, and t_c) were randomly varied over the ensemble. For each member of the ensemble, Γ_{ij} and its descendants were computed using two different upper frequency limits for the inner product in (11). In one case, the integral was truncated at the Schwarzchild inner-most stable circular orbit (ISCO) frequency whereas in the second case it was continued for an order of magnitude past the peak (merger) frequency. The goal was to estimate the impact of the post-ISCO portions of the waveform on parameter estimation. Table 1 lists the mean and median values of the SNR and parameter errors for the ensemble. Histograms of each parameter error for both cases are shown in Figure 1.

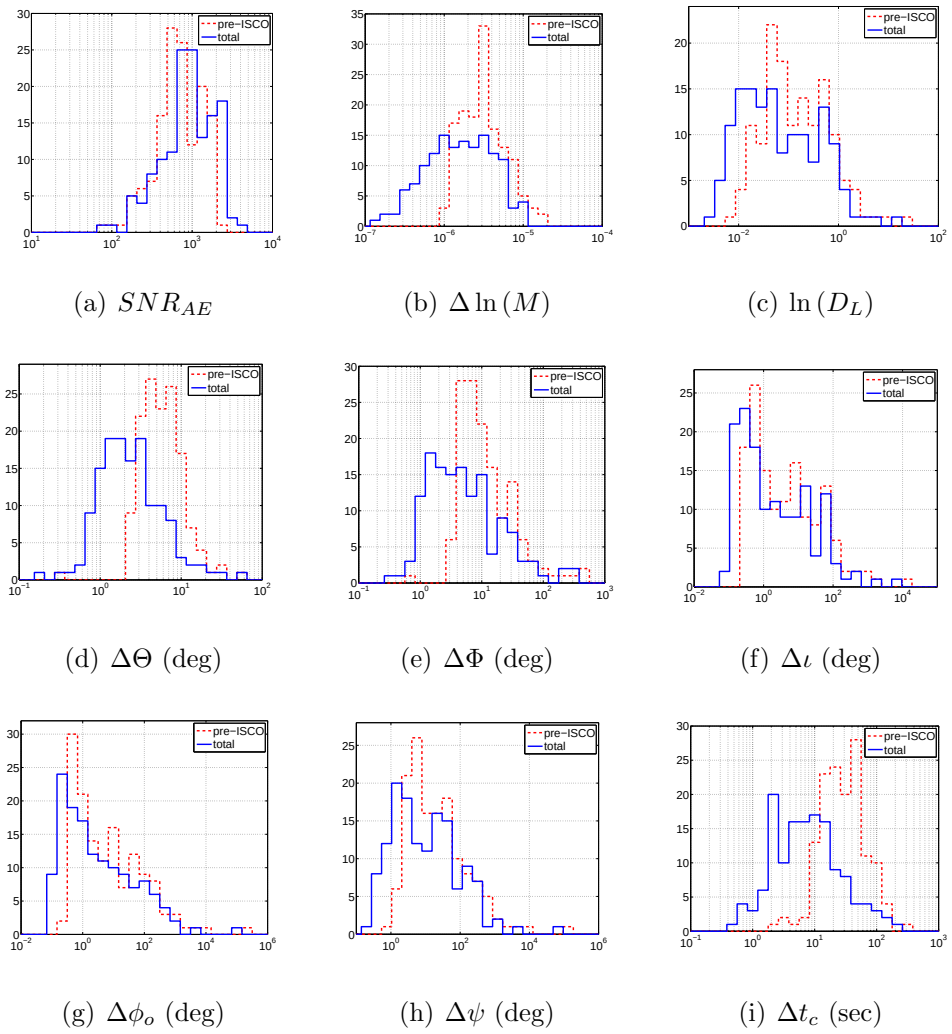

(a) SNR_{AE} (b) $\Delta \ln(M)$ (c) $\ln(D_L)$

(d) $\Delta\Theta$ (deg) (e) $\Delta\Phi$ (deg) (f) $\Delta\iota$ (deg)

(g) $\Delta\phi_o$ (deg) (h) $\Delta\psi$ (deg) (i) Δt_c (sec)

Figure 1. Histograms for SNR and parameter errors for an ensemble of 140 equal-mass, non-spinning binaries with $M = 10^6\,\mathrm{M}_\odot$ at $D_L = 6\,\mathrm{Gpc}$ ($z \sim 1$). For the 'pre-ISCO' case, the integration of Fisher matrix elements was cutoff at a frequency corresponding to the Schwarzchild ISCO. The 'total' case includes the entire waveform.

For each of the parameters there is a clear reduction in error when the post-ISCO portion of the waveform is included. The median improvement is about a factor of two, with the exception of the coalescence time, which improves by a factor of roughly four. In all cases, the improvement factor is greater than the median improvement in SNR of $\sim$25%, suggesting that most of the improvement is via a mechanism other than direct increase in SNR.

One possible mechanism is that a pair of parameters that is nearly degenerate in the inspiral phase become decoupled in the more complex merger phase of the waveform. Table 2 lists the percentage decrease in covariance for each parameter pair from pre-ISCO to total waveform. Note that all of the covariances decrease when the post-ISCO waveform is added. Covariances with the coalescence time exhibit the most dramatic decrease. This can be qualitatively explained by arguing that the merger provides a

Table 2. Median percentage reduction in covariance from pre-ISCO to total signal, $1 - \Sigma_{ij}^{(total)}/\Sigma_{ij}^{(pre-ISCO)}$.

	$\ln M$	$\ln D_L$	Θ	Φ	ι	ϕ_o	ψ	t_c
$\ln M$	72.3	70.8	63.5	90.7	71.4	79.2	82.4	91.1
$\ln D_L$	-	75.7	79.6	82.3	76.4	83.5	83.4	95.4
Θ	-	-	80.9	89.6	80.8	77.2	81.9	97.6
Φ	-	-	-	82.9	83.1	80.8	81.8	87.2
ι	-	-	-	-	76.8	87.0	86.6	94.8
ϕ_o	-	-	-	-	-	78.7	78.5	91.8
ψ	-	-	-	-	-	-	78.3	93.0
t_c	-	-	-	-	-	-	-	94.2

sharp feature that constrains the coalescence time more tightly and breaks degeneracies with other parameters.

3.1. Evolution of Parameter Errors

The results in Table 1, Figure 1, and Table 2 demonstrate the improvement in parameter estimation when the merger and ringdown portions of the waveform are included. A related question is to ask how the parameter information accumulates with time. This is of great interest to the problem of searching for electromagnetic (EM) counterparts for MBHB mergers. If the EM counterpart is nearly simultaneous with the peak of the GW signal and is short-lived, it is critical to have advance information as to the location of the merger in order to assist the EM search.

Figure 2 shows the effect of varying the upper cutoff frequency of the inner product in (11) on the SNR as well as the errors ΔD_L, $\Delta\Theta$, and $\Delta\Phi$. From the an EM counterpart search perspective, these (along with perhaps t_c) are the most critical parameters. For equal mass systems that are dominated by quadrupolar radiation, the upper cutoff frequency is a reasonable proxy for time before merger. During the inspiral phase, the two can be related using PN expressions[17]. Included on the plots in Figure 2 are points corresponding to times one minute, one hour, one day, and one week before merger.

The evolution of parameter errors in Figure 1 demonstrate the importance of the latter portions of the inspiral and the merger signal. The sky positions each improve by more than an order of magnitude in the final day of the signal. For comparison, Lang & Hughes[18] looked at spinning, precessing, unequal mass binaries in the post-Newtonian regime and found that sky position error decreased by similar amount during the final day before merger. Such behavior may influence the design of LISA mission operations. If the final days and hours of a signal are the most important in terms of source localization there will be pressure to reduce the latency between LISA and electromagnetic observatories. This could effect decisions on data downlink operations, inter-spacecraft communications, and other aspects of the mission.

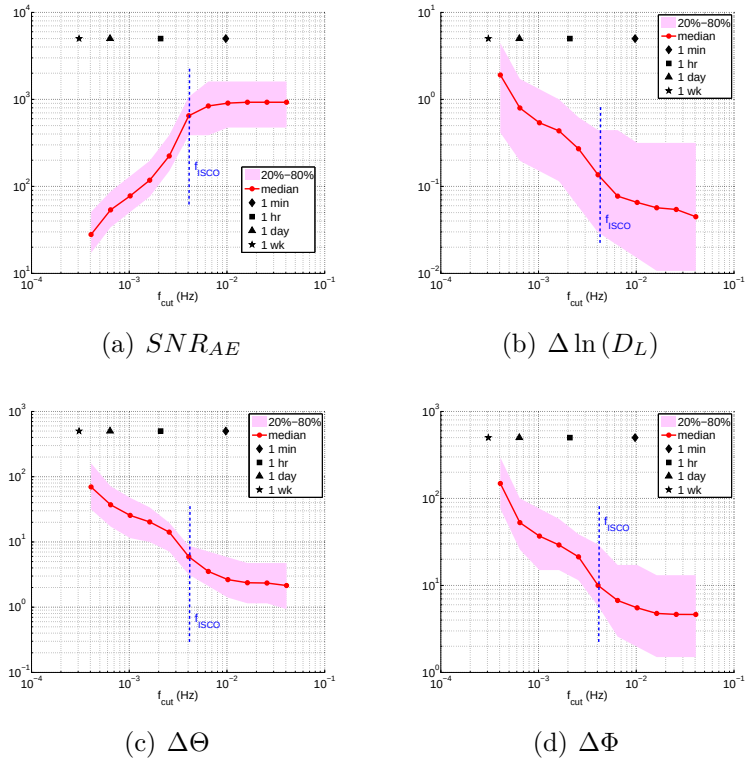

(a) SNR_{AE} (b) $\Delta \ln (D_L)$

(c) $\Delta\Theta$ (d) $\Delta\Phi$

Figure 2. Effect of upper frequency cut on SNR and source location errors for an ensemble of 140 equal-mass, non-spinning MBHBs with $M = 10^6\,\mathrm{M}_\odot$ and $D_L = 6\,\mathrm{Gpc}$. The filled circles denote the median values while the shaded area gives the range of the 20^{th} to 80^{th} percentile. The vertical dashed line denotes the Schwarzchild ISCO frequency, 4.4 mHz for these parameters. The individual solid markers denote time before merger.

3.2. Effect of Mass

As a test of the effect of total redshifted system mass on our parameter estimation results, we repeated our Monte Carlo run using an ensemble of 140 equal-mass, non-spinning MBHBs with $M = 10^7\,\mathrm{M}_\odot$ and $D_L = 6\,\mathrm{Gpc}$. Table 3 gives a summary of the mean and median parameter errors for this run. Comparing with the analogous ensemble of $M = 10^6\,\mathrm{M}_\odot$ systems summarized in Table 1, the heavier systems generally exhibit a reduced SNR and increased parameter errors. This is to be expected given the fact that the GW signal is shifted to lower frequencies and consequently is more obscured by the steeply-rising acceleration noise in the LISA detector. As with the $M = 10^6\,\mathrm{M}_\odot$ systems, the reduction in parameter errors with the inclusion of the merger signal is still present in the $M = 10^7\,\mathrm{M}_\odot$ case.

4. Conclusion

The results in section 3 give an indication as to the effect of the merger portion of the waveform on LISA's ability to measure source parameters. Making a precise comparison

Table 3. Mean ($\Delta\bar{\lambda}^i$) and median ($\Delta\tilde{\lambda}^i$) values for parameter errors for an ensemble of 140 equal-mass, non-spinning binaries with $M = 10^7\,\mathrm{M}_\odot$ at $D_L = 6\,\mathrm{Gpc}$ ($z \sim 1$). For the 'pre-ISCO' case, the integration of Fisher matrix elements was cutoff at a frequency corresponding to the Schwarzchild ISCO. The 'total' case includes the entire waveform.

λ^i	$\Delta\bar{\lambda}^i$ (total)	$\Delta\bar{\lambda}^i$ (pre-ISCO)	$\Delta\tilde{\lambda}^i$ (total)	$\Delta\tilde{\lambda}^i$ (pre-ISCO)
SNR_{AE}	98.5	26.8	85.2	22.9
$\ln(M/M_\odot)$	1.55×10^{-6}	2.66×10^{-6}	1.01×10^{-6}	1.89×10^{-6}
$\ln(D_L/1\,\mathrm{pc})$	2.17	2.83	8.04×10^{-1}	1.07
Θ (deg)	22.4	33.5	19.8	27.6
Φ (deg)	58.4	103	22.0	35.1
ι (deg)	9.65	25.2	5.88×10^{-1}	1.40
ϕ_o (deg)	1.58×10^3	2.80×10^3	33.3	43.9
ψ (deg)	1.62×10^3	2.87×10^3	79.9	111
t_c(sec)	14.7	77.2	13.1	68.5

with previous estimates is complicated by the fact that different physics is included in the source waveforms and different sets of parameters are used to describe them. Two of the most commonly-quoted parameters are the fractional luminosity distance $\Delta D_L/D_L \approx \Delta \ln(D_L)$ and the solid angle subtended by the error ellipse, $\Delta\Omega_N$. The latter quantity can be computed (REF Lang & Hughes) from the sky position angles, their errors, and their covariance.

In Table 4, $\Delta D_L/D_L$ and $\Delta\Omega_N$ from our ensemble of systems with $M = 10^6\,\mathrm{M}_\odot$ at $z \approx 1$ are compared with results from prior published works. Aside from the differences in the waveform physics (spin, merger, etc.), the biggest difference in the studies is that the length of the waveforms in this work are a factor of ~ 30 shorter than those used in the other published works. This is primarily due to the computational effort required to simulate long waveforms with *Synthetic LISA*.

The best comparison that can be made with this work is to compare the non-spinning results of Cutler and of Vecchio to our pre-ISCO case. $\Delta D_L/D_L$ is a factor of $2 \sim 5$ larger in our results than the published results. When the merger is added, the three results for $\Delta D_L/D_L$ approximately agree. This suggests that observing the final $\sim 10\,\mathrm{days}$ of a $M = 10^6\,\mathrm{M}_\odot$ MBHB at $z \sim 1$ will constrain D_L equally as well as observing the entire year prior to ISCO.

The results for $\Delta\Omega_N$ for the short waveforms are considerably worse. This indicates that the modulation imposed by the LISA orbits plays an important role in determining these parameters, a suggestion that agrees with the model proposed by Cutler. Nevertheless, the improvement in $\Delta\Omega_N$ upon inclusion of the merger is a factor of ~ 5, roughly the same factor as the inclusion of spin precession. Whether this same level of improvement will persist when the merger portion of the waveform is combined with long-duration observations, spin, and precession will depend on the

Table 4. Comparison of source location for equal-mass MBHBs at $z \sim 1$ in this work to prior published works.

	$M\,(10^6\,\mathrm{M}_\odot)$	duration (yr)	spin	precession	merger	$\Delta\Omega_N$ (deg^2)	$\Delta D_L/D_L$
Cutler[4]	4.0	1.0	no	no	no	$4 \times 10^{-1*}$	$7 \times 10^{-2*}$
Vecchio[5]	4.0	1.0	no	no	no	$6 \times 10^{-1\dagger}$	$2 \times 10^{-2\dagger}$
Vecchio[5]	4.0	1.0	yes	no	no	$3 \times 10^{-1\dagger}$	$6 \times 10^{-3\dagger}$
Lang & Hughes[18]	1.2	$\sim$1.5 (avg)	yes	yes	no	5.56×10^{-2}	3.57×10^{-3}
this work	1.0	0.03	no	no	no	5.08×10^{1}	1.18×10^{-1}
this work	1.0	0.03	no	no	yes	1.13×10^{1}	4.48×10^{-2}

*Estimated from the results in Table II in [4]

†Estimated from histograms in FIG. 2 in [5]

exact mechanism by which the improvement arises. If both improvements result from breaking the same parameter degeneracy, then the improvements will add rather than multiply. In other words, you can't break the same degeneracy twice. If however, the mechanisms for improvement are different, it is possible that the relative improvement when including the merger will be similar to the case here.

In summary we have found that inclusion of the merger signal in equal-mass, non-spinning MBHB waveforms can reduce errors in LISA parameter estimation by factors of a few over analyses that include the merger only. We expect that this improvement will persist as other effects such as unequal masses, spins, and higher harmonics are included.

Acknowledgments

This research was supported by an appointment to the NASA Postdoctoral Program at the Goddard Space Flight Center, administered by Oak Ridge Associated Universities through a contract with NASA.

References

[1] P. Bender, K. Danzmann, and the LISA Study Team. Laser interferometer space antenna for the detection of graviational waves, pre-phase a report. Technical Report MPQ233, Max-Planck-Institut fur Quantenoptik, Garching, 1998. 2nd ed.

[2] M. Volonteri. Supermassive black hole mergers and cosmological structure formation. In S.M. Merkowitz and J.C. Livas, editors, *Proceedings of the Sixth International LISA Symposium*, volume 873. American Institute of Physics, 2006.

[3] D. E. Holz and S.A. Hughes. Using gravitational-wave standard sirens. *Ap.J.*, 629:15–22, 2005.

[4] C. Cutler. Angular resolution of the lisa gravitational wave detector. *Phys. Rev. D*, 57:7089–7102, 1998.

[5] A. Vecchio. Lisa observations of rapidly spinning massive black hole binary systems. *Phys. Rev. D*, 70(042001), 2004.

[6] R.N. Lang and S.A. Hughes. Measuring coalescing massive black hole binaries: The impact of spin-induced precession. *Phys. Rev. D*, 74(122001), 2006.

[7] E.K. Porter and N.J. Cornish. The effect of higher harmonic corrections on the detection of massive black hole binaries with lisa. *Phys. Rev. D*, 78(064005), 2008.

[8] J.G. Baker, J. Centrella, D.-I. Choi, M Koppitz, and J. van Meter. Binary black hole merger dynamics and waveforms. *Phys. Rev. D*, 73(104002), 2006.

[9] M. Campanelli, C.O. Lousto, and Y. Zlochower. The last orbit of binary black holes. *Phys. Rev. D*, 73(061501(R)), 2006.

[10] J.G. Baker, S.T. McWilliams, J.R. van Meter, J. Centrella, D. Choi, B.J. Kelly, and M. Koppitz. Binary black hole late inspiral: Simulations for gravitational wave observations. *Phys. Rev. D*, 75(124024), 2007.

[11] S.L. Larson. Unequal arm space-born gravitational wave detectors. *Phys. Rev. D*, 66(062001), 2002.

[12] M. Tinto and J.W. Armstrong. Cancellation of laser noise in an unequal arm interferometer detector of gravitational radiation. *Phys. Rev. D*, 59(102003), 1999.

[13] F.B. Estabrook, M. Tinto, and J.W. Armstrong. Time-delay analysis of lisa gravitational wave data: Elimination of spacecraft motion effects. *Phys. Rev. D*, 62(042002), 2000.

[14] T.A. Prince, M. Tinto, S.L. Larson, and J.W. Armstrong. Lisa optimal sensitivity. *Phys. Rev. D*, 66(122002), 2002.

[15] M. Vallisneri. Synthetic lisa: Simulating time delay interferometry in a model lisa. *Phys. Rev. D*, 71(022001), 2005.

[16] S.E. Timpano, L.J. Rubbo, and N.J. Cornish. Characterizing the galactic gravitational wave background with lisa. *Phys. Rev. D*, 73(122001), 2006.

[17] L. Blanchet. Gravitational radiation from post-newtonian sources and inspiraling compact binaries. *Living Rev. Relativity*, 9(4), 2006.

[18] R.N. Lang and S.A. Hughes. Localizing coalescing massive black hole binaries with gravitational waves. *Ap.J.*, 677(2):1184–1200, 2008.